International Core Journal of Engineering Volume 12 Issue 4, 2026
ISSN: 2414-1895 DOI: 10.6919/ICJE.202604_12(4).0019

High-Temperature Mechanical Properties and Fracture Mechanisms of $FeNiCo(AlSi)_x$ High-Entropy Alloys

Zhe Li

College of Mechanical Engineering, Tianjin University of Technology and Education, Co 30000, Tianjin, China

Abstract

High-entropy alloys(HEAs)have attracted considerable attention as next-generation structural materials owing to their exceptional combination of mechanical properties and elevated-temperature stability.In this study,we systematically investigated the high-temperature microstructural evolution,compressive and tensile mechanical behavior,and fracture mechanisms of $FeNiCo(AlSi)_x$(x=0.1–0.6)HEAs at 400 °C.Ingots were synthesized by vacuum induction levitation melting and homogenized at 1000°C for 4 hours.With increasing AlSi content,a progressive FCC-to-BCC structural transition was confirmed,with the critical two-phase coexistence zone identified near x=0.3.At 400 °C,the x=0.1 alloy exhibited anomalous high-temperature strengthening with a compressive strength of approximately 3075 MPa,attributed to dynamic strain aging and dynamic recovery operating synergistically within the continuous FCC matrix.Alloys with x≥0.3 underwent severe high-temperature embrittlement driven by thermally accelerated B2 phase precipitation,with fracture modes transitioning progressively from ductile dimple rupture to transgranular and intergranular brittle cleavage.The composition x=0.2 demonstrated the most favorable overall high-temperature mechanical performance,providing critical design guidelines for FeNiCo-based structural applications in elevated-temperature service environments.

Keywords

High-entropy Alloys; FCC-to-BCC Phase Transformation; High-temperature Mechanical Properties; Fracture Mechanisms; Dynamic Strain Aging.

1. Introduction

The design philosophy underlying conventional structural alloys has historically been anchored in a single principal element matrix,augmented by carefully selected minor alloying additions that confer specific thermomechanical advantages.This paradigm has underpinned the development of some of the most successful engineering materials in modern history,including austenitic stainless steels,nickel-based superalloys,and titanium alloys,each optimized within tightly constrained compositional windows and deeply understood microstructural frameworks.However,the relentlessly escalating performance demands of contemporary aerospace propulsion,advanced power generation,and hypersonic structural applications are pushing conventional alloy systems toward their intrinsic physical limits.At elevated operational temperatures,single-principal-element matrices are fundamentally vulnerable to rapid elemental diffusion,precipitate coarsening,grain boundary weakening,creep deformation,and progressive microstructural degradation,all of which collectively erode load-bearing capacity and fracture resistance in service.These insurmountable limitations have catalyzed a sustained global research effort to identify radically novel alloy design paradigms capable of simultaneously delivering high-temperature strength,microstructural stability,and fracture

ISSN: 2414-1895 DOI: 10.6919/ICJE.202604_12(4).0019

toughness across the demanding temperature regimes encountered in next-generation engineering systems.

The concept of high-entropy alloys,independently and almost simultaneously articulated by Yeh et al.[1] and Cantor et al.[2] in 2004,represented a genuine paradigm shift in physical metallurgy and alloy design.By incorporating five or more metallic elements in near-equimolar ratios as co-principal constituents rather than minor additions,this approach exploits the high configurational entropy of mixing to thermodynamically stabilize simple solid-solution phases-predominantly face-centered cubic(FCC)or body-centered cubic(BCC)structures-against the formation of complex,brittle intermetallic compounds.This stabilization mechanism fundamentally decouples alloy complexity from microstructural brittleness,opening an enormous unexplored compositional space for systematic exploration.As comprehensively reviewed by Miracle and Senkov [3] and George et al.[4],the defining characteristics of HEAs-encompassing severe lattice distortion from pronounced atomic size mismatch among multiple principal elements,sluggish diffusion kinetics arising from the highly complex local chemical environment,and the synergistic cocktail effect enabling non-linear property contributions-collectively confer properties unattainable through conventional alloy design.Of particular relevance to elevated-temperature structural applications,the sluggish diffusion effect intrinsic to HEA systems substantially retards grain coarsening,precipitate dissolution,and thermally driven phase instability at high homologous temperatures,thereby preserving microstructural integrity under conditions that would catastrophically degrade conventional engineering alloys [3].Within this broad HEA landscape,FeNiCo-based systems occupy a strategically important position.The equiatomic FeNiCo ternary alloy naturally stabilizes a continuous,single-phase FCC solid solution across a wide compositional range,providing the geometric advantage of twelve independent slip systems-satisfying the von Mises criterion for arbitrary plastic deformation-and inherently low stacking fault energy effects that promote both dislocation glide and deformation twinning.These characteristics endow FeNiCo-based HEAs with high intrinsic ductility and deformation tolerance,establishing a resilient foundation upon which targeted compositional modifications can be applied to engineer high-temperature strengthening without sacrificing the fracture resistance that defines their engineering utility.

The mechanical behavior and microstructural characteristics of FeNiCo-based and related FCC-structured HEAs at both ambient and elevated temperatures have been documented extensively in the literature,providing essential mechanistic benchmarks.The landmark investigation by Gludovatz et al.[5] demonstrated that the equiatomic CrMnFeCoNi Cantor alloy achieves fracture toughness values exceeding 200 $MPa \cdot m^{1/2}$ at cryogenic temperatures due to thermally activated nanotwinning,establishing the FCC HEA system as an exceptional damage-tolerant structural material.Otto et al.[6] subsequently characterized the tensile mechanical behavior of CoCrFeMnNi across a temperature range spanning 77 K to 1073 K,demonstrating that strength decreases with increasing temperature while ductility is maintained through the activation of multiple thermally assisted dislocation recovery mechanisms.This foundational study established the primary limitation of FCC-dominant HEAs-namely,pronounced high-temperature softening-and underscored the critical need for compositional strategies to counteract thermal strength degradation.

The introduction of aluminum as a primary structural modifier into FCC-based HEAs has been recognized as the most potent and systematically exploited strategy for inducing FCC-to-BCC phase transformations and enhancing room-temperature and high-temperature strength.Wang et al.[7] established through a systematic compositional study that increasing Al content in Al_xCoCrFeNi alloys progressively destabilizes the FCC solid solution by reducing the valence electron concentration below the threshold required for FCC stability,driving a continuous structural transition through a dual-phase FCC + BCC coexistence region toward a fully BCC structure.The concurrent formation of B2-ordered Al-Ni-rich precipitates within the BCC matrix introduces additional strengthening through coherency strain hardening and ordered-domain boundary resistance to dislocation penetration.The role of silicon as a co-alloying element with aluminum has received comparatively less systematic attention,though critical studies have highlighted its unique

ISSN: 2414-1895 DOI: 10.6919/ICJE.202604_12(4).0019

contributions.Ma et al.[8] demonstrated that Si additions modify the valence electron concentration and atomic packing efficiency in CoCrFeNi-based alloys,fine-tuning the FCC/BCC phase boundary position with high sensitivity.Wang et al.[9] further showed that Si co-additions to Al_xCoCrFeNi alloys accelerate the FCC-to-BCC transition relative to Al addition alone,primarily through enhanced lattice strain accumulation arising from the pronounced atomic size mismatch of Si,while simultaneously increasing room-temperature hardness through solid-solution strengthening contributions.

The high-temperature mechanical response of HEAs is governed by a complex interplay of thermally activated strengthening and softening mechanisms whose relative contributions are highly sensitive to alloy composition and microstructural state.He et al.[10] elegantly demonstrated that coherent $L1_2$ nanoprecipitates in a$(NiCoFeCr)_{94}Al_3Ti_3$ HEA provide precipitation hardening with a yield strength exceeding 1 GPa at room temperature while retaining significant strength at 700 °C,establishing the critical role of ordered precipitate morphology and volume fraction in dictating high-temperature load-bearing capacity.Zhao et al.[11] subsequently provided quantitative characterization of the thermal coarsening kinetics of coherent B2 and $L1_2$ particles in precipitation-hardened HEAs,demonstrating that coarsening rates are substantially slower than in conventional Ni-based superalloys due to sluggish elemental diffusion,with critical implications for the long-term high-temperature stability of precipitate-strengthened HEA systems.At intermediate elevated temperatures,dynamic strain aging(DSA)emerges as a dominant strengthening mechanism through the thermally activated re-pinning of mobile dislocations by diffusing solute atoms.Luo et al.[12] identified DSA as operative in FeCoNiCr-based HEAs at temperatures between 300 °C and 600 °C,manifested through characteristic serrated flow phenomena and anomalous strength-temperature dependence.The concurrent operation of dynamic recovery-involving thermally activated dislocation climb,cross-slip,and annihilation-can delocalize plastic deformation and delay fracture initiation [6,13],producing a temperature regime in which strength and ductility are simultaneously preserved.

The fracture behavior of compositionally complex alloys at elevated temperatures has been systematically characterized by Zhang et al.[14],who documented the critical dependence of fracture mode on phase constitution and grain boundary chemistry,identifying that the transition from ductile dimple rupture to intergranular brittle fracture is strongly correlated with Al and Si grain boundary segregation in BCC-dominant compositions.Senkov et al.[15] further established in refractory HEA systems that elevated-temperature fracture resistance is critically governed by the balance between grain boundary cohesion energy and the local stress state imposed by mismatch between constituent phases,providing mechanistic principles broadly applicable to transition-metal HEA systems.Additional insights from George et al.[16] and Miracle and Senkov [3] collectively underscore that quantitative,mechanism-resolved composition–microstructure–property frameworks represent the essential foundation for translating HEA discoveries into engineering applications.Wu et al.[17] provided quantitative solid-solution strengthening models explicitly validated for FCC multi-component alloys,demonstrating that atomic-scale lattice friction stress is substantially elevated in HEAs relative to binary alloys due to the statistical distribution of local chemical environments encountered by gliding dislocations,a contribution that becomes increasingly significant at elevated temperatures as the competing thermal softening of the lattice modulus is partially offset by solute–dislocation interaction strengthening.

Despite the growing body of literature on FCC-to-BCC transitions and high-temperature mechanical behavior in Al-containing HEAs,a comprehensive and quantitative investigation specifically targeting the coupled effects of AlSi co-additions across the full composition range of the $FeNiCo(AlSi)_x$ system(x=0.1–0.6)at elevated temperatures remains absent from the published literature.In particular,the mechanistic attribution of anomalous high-temperature strengthening phenomena,the quantification of fracture mode transitions driven by thermally activated B2 phase precipitation,and the identification of optimal compositional windows for high-temperature structural applications have not been systematically established for this alloy family.We therefore present in

ISSN: 2414-1895 DOI: 10.6919/ICJE.202604_12(4).0019

this work a comprehensive experimental investigation of high-temperature microstructural evolution,compressive and tensile mechanical behavior at 400 °C,and fracture mechanism characterization for the complete $FeNiCo(AlSi)_x$ alloy series.Our principal objectives are as follows: first,to elucidate the microstructural state of each alloy composition at 400 °C,explicitly characterizing the phase constitution,precipitate morphology,and grain boundary character;second,to quantify the high-temperature compressive and tensile mechanical parameters-including yield strength,flow stress,elastic modulus,maximum strain,and failure mode-across the full compositional range;third,to mechanistically rationalize the anomalous high-temperature strengthening observed at x=0.1 through the combined framework of dynamic strain aging and dynamic recovery;fourth,to establish the microstructural origins of progressive high-temperature embrittlement at x≥0.3 through systematic fractographic analysis;and fifth,to identify the optimal AlSi content window for balancing high-temperature strength,ductility,and fracture resistance in FeNiCo-based structural applications.Our findings provide a quantitative composition–microstructure–property framework that directly informs compositional design decisions for $FeNiCo(AlSi)_x$ HEAs intended for deployment in elevated-temperature structural environments.

2. Literature References

We designed and synthesized six $FeNiCo(AlSi)_x$ alloy compositions with x=0.1,0.2,0.3,0.4,0.5,and 0.6 based on atomic molar ratios.In this compositional framework,the Fe,Ni,and Co base elements were maintained at a strictly equiatomic ratio of 1:1:1,while Al and Si were co-introduced as alloying additions at a fixed Al:Si atomic ratio of 1:1.The systematically varied total AlSi molar ratio x constitutes the primary independent compositional variable across the alloy series.The specific atomic percentages and corresponding mass fractions for all six alloy compositions are summarized in Table 1 providing the precise formulation basis for each alloy investigated.

Table 1. Physical Parameters of Experimental Materials

Element	Purity (%)	Melting Point (℃)	VEC	Atomic Radius (pm)	Structure
Fe	≥99.9	1539	8	124	BCC
Ni	≥99.9	1455	9	125	FCC
Co	≥99.9	1495	10	125	HCP
Al	≥99.9	660	3	143	FCC
Si	≥99.9	1414	4	117	Diamond

Prior to alloy synthesis,all elemental raw materials-including Fe,Ni,Co,Al,and Si particles of purity≥99.9 wt.%-were subjected to a rigorous pre-treatment protocol to eliminate surface-adsorbed moisture and organic contaminants that could degrade the chemical integrity of the fabricated ingots.Specifically,all raw materials were dried in a vacuum oven at 120 °C for 4 hours to physically desorb atmospheric moisture,followed by ultrasonic cleaning in anhydrous ethanol for 15 minutes to remove residual surface oils and microcontaminants,and subsequently dried at 60 °C under forced convection.Elemental masses corresponding to the target atomic compositions were then precisely calculated and weighed using a high-precision analytical balance(FA2004N)accurate to 0.1 mg,with each ingot formulated to a standardized total mass of 150 ± 5 g to ensure consistent melt pool volumes and minimize processing variability across the alloy series.Unused raw materials were stored under vacuum to prevent recontamination.

Alloy ingots were produced using a VLF500 vacuum induction levitation melting furnace operating under high-vacuum conditions.This technique exploits electromagnetic induction to levitate and melt the constituent metals within a coil-generated magnetic field,entirely eliminating crucible wall contact and the associated risk of refractory contamination.The intense electromagnetic stirring intrinsic to the levitation process promotes thorough melt convection and homogenization of the

ISSN: 2414-1895 DOI: 10.6919/ICJE.202604_12(4).0019

liquid alloy,substantially reducing compositional segregation in the solidified ingot relative to conventional induction melting with a ceramic crucible.Each alloy charge was subjected to a minimum of three repeated melt-and-solidify cycles under vacuum to further enhance chemical homogeneity and ensure complete dissolution of all constituent elements.The resulting as-cast ingots were subsequently subjected to homogenization heat treatment in a muffle furnace(SX2-12-10)at 1000 °C for 4 hours.This thermal processing step was designed to eliminate residual dendritic microsegregation,dissolve non-equilibrium low-melting-point phases formed during rapid solidification,and establish a chemically uniform solid-solution microstructure as the baseline condition for all subsequent characterization and testing.

Mechanical test specimens and characterization coupons were extracted from the central regions of the homogenized ingots using a precision wire electrical discharge machining tool(DK7732)to avoid the introduction of thermomechanical surface damage or residual stresses associated with conventional abrasive cutting.For microstructural characterization,the specimen surfaces were prepared by sequential mechanical grinding through 400,800,1200,and 2000 grit silicon carbide abrasive papers on a metallographic polishing machine(MP-2B),followed by fine polishing using 3 μm and 1 μm diamond suspension,and a final vibratory polishing step in 0.05 μm colloidal silica suspension for a minimum of 4 hours to achieve a mechanically strain-free,mirror-quality surface suitable for electron backscatter diffraction analysis.

Phase identification and lattice parameter determination across the alloy composition series were carried out by X-ray diffraction(XRD)using a Rigaku Ultima IV diffractometer with Cu-Kα radiation(λ=0.15406 nm),scanning over a 2θ range of 20° to 100° at a step size of 0.02° and a scanning speed of 2°/min.Diffraction patterns were analyzed using MDI Jade software with reference to the ICDD powder diffraction database for phase indexing and identification.Microstructural morphology,second-phase distribution,and elemental partitioning were characterized using a JEOL JSM-7100F field-emission scanning electron microscope(SEM)operating in both secondary electron(SE)and backscattered electron(BSE)imaging modes.BSE imaging was employed primarily for metallographic cross-sections to exploit atomic number contrast for phase-sensitive imaging,while SE imaging was applied exclusively for post-deformation fracture surface examination to resolve fine topographic features of the failure surfaces.Energy-dispersive X-ray spectroscopy(EDS)was performed in conjunction with SEM imaging for quantitative point analysis and elemental mapping of matrix and precipitate phases.High-resolution crystallographic orientation mapping and phase distribution analysis were conducted using EBSD,with data acquired at 20 kV accelerating voltage and step sizes of 0.2–0.5 μm adjusted according to local microstructural length scale.EBSD data post-processing employed the HKL Channel 5 software suite for inverse pole figure(IPF)map generation,phase map construction,and kernel average misorientation(KAM)analysis to assess local plastic strain accumulation.

For elevated-temperature microstructural characterization representative of the 400 °C service condition,selected specimens were subjected to isothermal heat treatment at 400 °C for durations matching the mechanical test thermal exposure profile,followed by immediate water quenching to arrest the high-temperature microstructural state.This quench-and-characterize approach provides a reliable approximation of the in-service microstructural condition,given the substantially sluggish diffusion kinetics in $FeNiCo(AlSi)_x$ HEAs that limit microstructural evolution during the quenching transient.The high-temperature phase transformation behavior was further characterized by simultaneous differential scanning calorimetry and thermogravimetric analysis(DSC-TGA)using a TA Instruments SDT Q600 thermal analyzer,with specimens heated from room temperature to 1200°C at a heating rate of 10 °C/min under flowing argon to identify phase transformation temperatures,precipitation event temperatures,and sample mass stability.

Elevated-temperature mechanical properties were evaluated by uniaxial compression testing at 400 °C using an E45.105 electronic universal testing machine equipped with an integrated high-temperature environmental furnace chamber.Cylindrical compression specimens with standardized

ISSN: 2414-1895 DOI: 10.6919/ICJE.202604_12(4).0019

dimensions of Φ3 mm × 6 mm(diameter × height,aspect ratio 2:1)were machined for all compression evaluations.For the tensile investigation,which was focused on the most promising compositions(x=0.1 and x=0.2)identified from room-temperature compression screening,dog-bone shaped specimens with a gauge length of 10 mm,width of 3 mm,and thickness of 1.5 mm were fabricated.For all elevated-temperature mechanical tests,specimens were heated to 400 °C at a controlled rate of 10 °C/min and held isothermally for 15 minutes prior to mechanical loading initiation to ensure complete and uniform thermal equilibration throughout the specimen cross-section.Boron nitride-based lubricant was applied to the compression platens to minimize friction-induced barreling artifacts during compressive deformation.All mechanical tests were conducted at a constant initial engineering strain rate of 1×10^{-3} s^{-1},with engineering stress and engineering strain recorded in real time using a calibrated load cell and video extensometer respectively.A minimum of three independent parallel tests were performed for each composition and temperature condition,with mean values and associated standard deviations reported throughout this work to ensure statistical reliability of all quantitative results.

Following mechanical testing,fracture surfaces of ruptured specimens were preserved without further mechanical preparation and examined directly under SE imaging in the SEM to characterize the operative fracture mechanisms with full topographic fidelity.Loose surface debris was removed by gentle nitrogen gas blowing prior to SEM examination.Quantitative mechanical property parameters-including compressive strength,elastic modulus,maximum compressive strain,and failure mode classification-were extracted from the stress–strain curves as documented in Table 2.Engineering stress–strain curves were processed and plotted using Origin 2023 software,while quantitative mechanistic calculations,including dislocation density estimates from XRD peak broadening analysis and precipitate size distribution statistics from SEM image processing,were performed using custom-developed Matlab scripts to provide a rigorous quantitative basis for the mechanistic interpretations presented in the Results and Discussion sections of this manuscript.

3. Results and Discussion

The XRD diffraction patterns for all $FeNiCo(AlSi)_x$ compositions following homogenization are presented in Figure 1.or x=0.1,the pattern exhibits exclusively FCC-phase characteristic reflections at 2≈44°,51°,75°,and 91°,corresponding to the(111),(200),(220),and(311)planes respectively,confirming complete dissolution of AlSi additions into the FeNiCo FCC solid solution matrix without detectable secondary phase formation.The progressive structural evolution with increasing x is systematic and clearly resolved.At x=0.2,the FCC reflection intensities attenuate measurably and peak positions shift slightly toward lower 2θ angles,indicating lattice parameter expansion driven by the substitutional accommodation of larger Al atoms(atomic radius 1.43Å)relative to the Fe,Ni,and Co host atoms,accompanied by peak broadening consistent with enhanced microstrain accumulation and incipient compositional fluctuations at the nanoscale.The critical structural transition is unambiguously identified at x=0.3,where emergent diffraction peaks at 2θ≈45° and 83° confirm the onset of BCC phase formation alongside weakening FCC reflections,establishing the two-phase FCC + BCC coexistence region.Additional superlattice reflections at positions consistent with B2 ordering further confirm the formation of chemically ordered Al-Ni-rich intermetallic domains at this composition.For x=0.4 through x=0.6,the BCC and B2 reflections progressively dominate the diffraction profiles while FCC signals diminish toward the detection threshold,confirming nearly complete phase transformation to BCC/B2 dual-phase microstructures at high AlSi contents.

ISSN: 2414-1895 DOI: 10.6919/ICJE.202604_12(4).0019

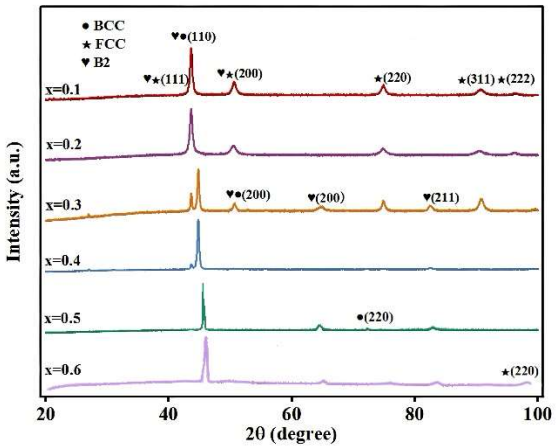

Figure 1. XRD Diffraction Pattern of $FeNiCo(AlSi)_x$ High-Entropy Alloy at 400°C

The microstructural morphology revealed by SEM imaging(Figure 2)provides direct visual corroboration of the phase transformation sequence established by XRD.

In the x=0.1 and x=0.2 alloys,the microstructure consists of equiaxed grains with homogeneous elemental distribution and no visible second-phase particles or interphase boundaries,consistent with single-phase FCC solid solutions.At x=0.3,a markedly distinct microstructure emerges,characterized by the formation of lamellar or plate-like secondary phases preferentially nucleated along grain boundaries and extending into the grain interiors.EDS point analysis identifies these secondary phases as Al- and Ni-enriched regions chemically consistent with the ordered B2(Ni,Co)Al intermetallic,confirming that the onset of B2 precipitation at x=0.3 occurs concurrently with the FCC-to-BCC transformation detected by XRD.

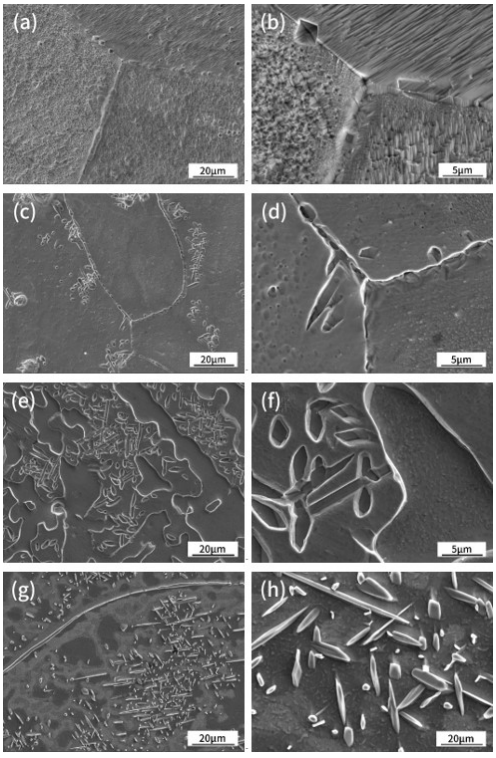

Figure 2. $FeCoNi(AlSi)_x$(x=0.1-0.4)Alloy SEM Images at 400°C
(a,b)x=0.1(c,d)x=0.2(e,f)x=0.3(g,h)x=0.4

ISSN: 2414-1895 DOI: 10.6919/ICJE.202604_12(4).0019

The EBSD inverse pole figure maps presented in Figure 3 and 4 that alloys with x≥0.4 develop a morphologically complex Widmanstätten-type microstructural arrangement in which the rigid B2 phase forms a continuous or semi-continuous grain boundary network,fundamentally transforming the deformation constraint architecture of the alloy and establishing the microstructural basis for the high-temperature embrittlement observed in mechanical testing.

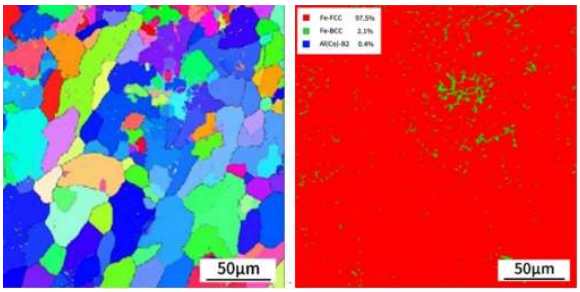

Figure 3. FeNiCo(AlSi)$_{02}$ Alloy 400°C EBSD Images
(a)Inverse Pole Figure(b)Image Quality Map

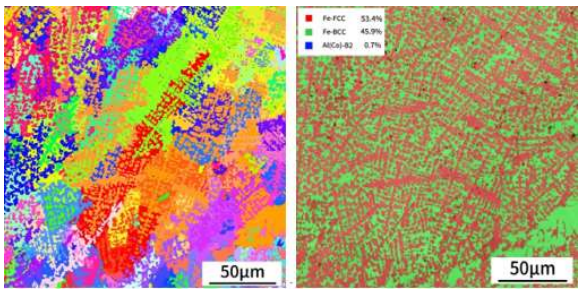

Figure 4. FeNiCo(AlSi)$_{0.3}$ Alloy 400°C EBSD mages
(a)Inverse Pole Figure(b)Image Quality Map

The high-temperature compressive stress–strain curves measured at 400 °C for all FeNiCo(AlSi)$_x$ compositions are presented in Figure 5,and the corresponding quantitative mechanical property parameters are summarized in Table 2.

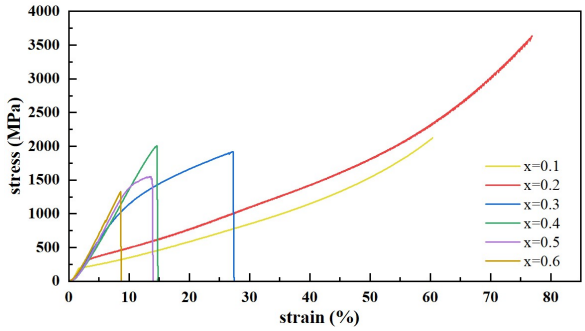

Figure 5. Stress-strain curve of FeNiCo(AlSi)$_x$ alloy at 400°C

The most striking result is the anomalous high-temperature strengthening exhibited by the x=0.1 alloy.Rather than the monotonic strength reduction with temperature that characterizes most structural alloys,the x=0.1 composition achieves a compressive strength of approximately 2123.95 MPa at 400 °C compared to 1787.28 MPa at room temperature,representing a positive temperature coefficient of strength that is mechanistically distinct from conventional thermal behavior.

ISSN: 2414-1895 DOI: 10.6919/ICJE.202604_12(4).0019

Table 2. Mechanical Properties Parameters of $FeNiCo(AlSi)_x$ at 400°C

T	X	Compressive Strength (MPa)	Elastic Modulus (GPa)	Maximum Strain (%)
400℃	x=0.1	2123.95	13.1	60.39
400℃	x=0.2	3634.34	5.5	76.89
400℃	x=0.3	1922.30	6.5	27.42
400℃	x=0.4	2004.49	3.35	14.78
400℃	x=0.5	1548.49	3.7	13.97
400℃	x=0.6	1327.36	8.0	8.69

We attribute this anomalous strengthening behavior to the synergistic operation of dynamic strain aging and dynamic recovery within the continuous FCC matrix.At 400 °C,the thermal activation energy is sufficient to mobilize Si and Al solute atoms,which diffuse toward and repetitively pin mobile dislocations during plastic deformation,generating an elevated effective flow stress through the Cottrell atmosphere pinning mechanism.The multi-solute nature of the $FeNiCo(AlSi)_x$ system provides a broad temperature window over which DSA is operative due to the diversity of solute diffusion activation energies,consistent with the documented behavior of analogous multi-solute HEA systems [12].

The concurrent dynamic recovery process-involving thermally activated dislocation climb and cross-slip-prevents excessive dislocation density accumulation and promotes deformation homogenization,allowing sustained plastic flow without premature fracture initiation.The macroscopic manifestation of these combined mechanisms is the preservation of substantial compressive plasticity(maximum strain 0.39%,consistent with the absence of visible macroscopic failure as documented in Table 2)alongside the elevated flow stress.

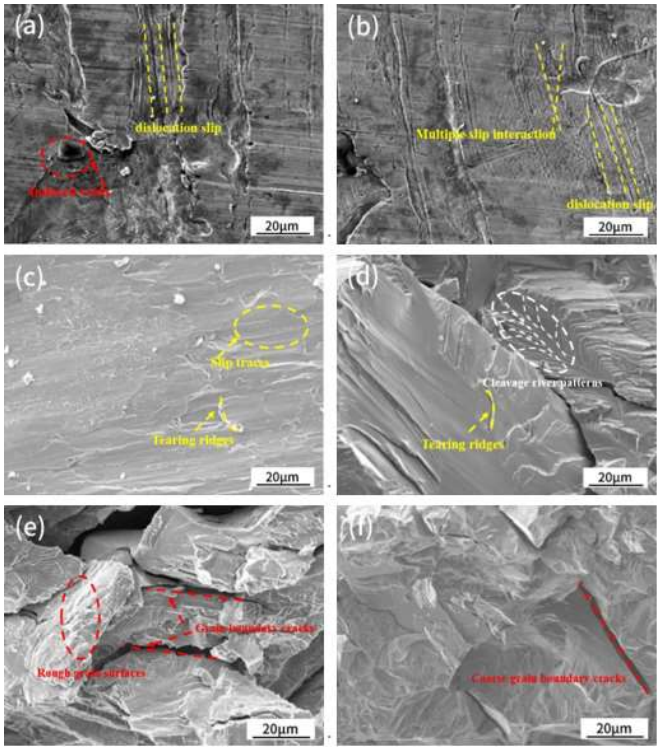

Figure 6. Compression fracture morphology of $FeNiCo(AlSi)_x$ allo at 400°C
(a)x=0.1,(b)x=0.2,(c)=0.3,(d)=0.4,(e)=0.5,(f)x=0.6

ISSN: 2414-1895 DOI: 10.6919/ICJE.202604_12(4).0019

The lateral morphology of the x=0.1 specimens post-compression(igure 6)confirms the maintenance of excellent plasticity through the presence of broadly distributed slip bands with rounded contours characteristic of thermally activated multi-system dislocation activity.

The x=0.2 alloy achieves the highest absolute compressive strength among all compositions at 400 °C,recording 3634.34 MPa at a maximum compressive strain of 6.89%,without evidence of macroscopic fracture(Table 2).

This superior high-temperature performance reflects the optimized combination of solid-solution strengthening-maximized by the higher AlSi content relative to x=0.1-and the retention of a predominantly continuous FCC matrix providing sufficient slip system availability to accommodate plastic deformation.The higher flow stress relative to x=0.1 is consistent with greater solid-solution hardening from more extensive lattice distortion,while the maintenance of significant plasticity reflects the preservation of FCC matrix connectivity that enables multi-system dislocation glide and stress redistribution during loading.

A dramatic deterioration in high-temperature mechanical performance is observed for x≥0.3.At x=0.3,the compressive strength drops to 1922.30 MPa with a maximum compressive strain of 7.42%,followed by a pronounced load drop indicating macroscopic structural instability(Table 2).For x=0.4,catastrophic post-peak load collapse occurs at 2004.49 MPa with maximum strain of 14.78%,and for x=0.5 and x=0.6,obvious brittle failure and strong brittle failure modes are documented at 1548.49 MPa and 1327.36 MPa respectively(Table 2).This progressive mechanical degradation with increasing AlSi content is inextricably linked to the thermally accelerated precipitation of coarse,continuous B2 phase networks at 400 °C.The DSC analysis confirms characteristic B2 precipitation exotherms commencing near 400 °C,confirming that this testing temperature corresponds to the onset of active B2 precipitation.During the isothermal thermal equilibration period preceding mechanical loading,thermodynamic driving forces accelerate B2 precipitate nucleation along grain boundaries,establishing a continuous brittle network that concentrates stress at phase boundaries and provides crack propagation paths of minimal resistance.The strain accommodation incompatibility between the plastically compliant FCC/BCC matrix and the rigid ordered B2 network generates interfacial stress concentrations that nucleate microcracks at critically low applied stresses,thereby eliminating the ductile deformation reservoir and precipitating early catastrophic failure.

The fractographic examination of specimens tested at 400 °C,presented in Figure 6,provides direct mechanistic evidence for the composition-dependent fracture mode transitions.

For x=0.1,the specimen maintains excellent macroscopic shape integrity without fracture,with slip traces visible on the specimen surface confirming widespread dislocation-mediated plastic deformation.The x=0.2 specimen similarly does not exhibit macroscopic fracture but shows pronounced lateral bulging,indicative of significant uniform compressive deformation distributed throughout the specimen volume.In sharp contrast,specimens with x=0.3 through x=0.6 exhibit unambiguous macroscopic fracture with progressively more brittle failure morphologies.At x=0.3,the fracture surface displays a mixed failure mode with localized dimpled regions interspersed with flat cleavage facets,consistent with a transitional fracture mechanism where competing ductile void growth and brittle cleavage operate in different microstructural domains.At x=0.5 and x=0.6,the fracture surfaces are characterized exclusively by flat,faceted intergranular fracture morphologies with characteristic river mark patterns,confirming that grain boundary B2 precipitation has embrittled the grain boundaries to the extent that intergranular crack propagation requires less energy than the alternative transgranular cleavage pathway.

The high-temperature tensile behavior further corroborates these composition-dependent mechanisms.As documented in Figure 7 the x=0.2 tensile specimen develops a well-defined necking zone prior to fracture,confirming significant plastic deformation capacity at 400 °C.The fracture surface of x=0.2(Figure 7b)reveals a characteristic mixed-mode fracture morphology: the central region exhibits shallow dimples consistent with void nucleation around B2 precipitates,while the

ISSN: 2414-1895 DOI: 10.6919/ICJE.202604_12(4).0019

peripheral region displays step-like cleavage features indicative of crack propagation along low-energy crystallographic planes.This mixed-mode character reflects the intermediate microstructural state of x=0.2 at 400 °C,wherein incipient B2 precipitation provides fine-scale dispersion hardening while insufficient in volume fraction to establish a continuous embrittling network,thereby preserving partial ductility alongside elevated strength.The transition from pure ductile to mixed-mode fracture between x=0.1 and x=0.2 is thus mechanistically attributable to the onset of B2 precipitate formation in the x=0.2 alloy,whose volume fraction and morphology at 400 °C remain below the critical threshold for continuous boundary embrittlement while still providing precipitate–dislocation interaction strengthening that elevates the flow stress above that achievable through solid solution strengthening alone.

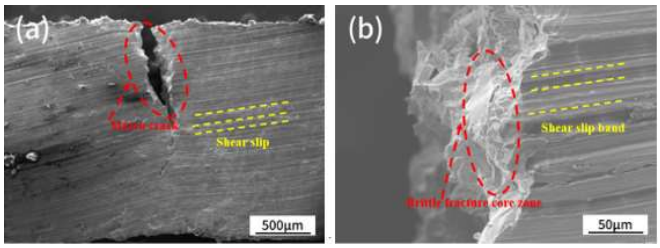

Figure 7 Tensile fracture morphology of $FeNiCo(AlSi)_{0.2}$ at 400℃

4. Conclusion

Collectively,our results establish a clear and quantitative composition–microstructure–high-temperature property framework for the $FeNiCo(AlSi)_x$ system.The FCC-to-BCC structural transition near x=0.3,driven by the BCC-stabilizing thermodynamic tendency of Al and the lattice strain contribution of Si,constitutes the critical compositional boundary separating high-temperature structural utility from severe embrittlement.Below this threshold,the combination of dynamic strain aging–induced strengthening and dynamic recovery–mediated ductility preservation enables exceptional high-temperature mechanical performance,with x=0.1 exhibiting the most remarkable anomalous strengthening and x=0.2 achieving the highest absolute strength while maintaining structural integrity.Above x=0.3,thermally accelerated B2 phase precipitation along grain boundaries fundamentally compromises high-temperature fracture resistance,producing a systematic deterioration in both strength and ductility that renders these compositions unsuitable for sustained high-temperature structural service.These findings provide concrete,mechanistically grounded compositional design guidelines for $FeNiCo(AlSi)_x$ HEAs,identifying the AlSi content window of x=0.1–0.2 as optimal for applications requiring the combined delivery of high-temperature strength,fracture toughness,and microstructural stability.

References

[1] Yeh,J.-W.et al.Nanostructured high-entropy alloys with multiple principal elements: novel alloy design concepts and outcomes.Adv.Eng.Mater.6,299–303(2004).

[2] Cantor,B.,Chang,I.T.H.,Knight,P.& Vincent,A.J.B.Microstructural development in equiatomic multicomponent alloys.Mater.Sci.Eng.A 375–377,213–218(2004).

[3] Miracle,D.B.& Senkov,O.N.A critical review of high entropy alloys and related concepts.Acta Mater.122,448–511(2017).

[4] George,E.P.,Raabe,D.& Ritchie,R.O.High-entropy alloys.Nat.Rev.Mater.4,515–534(2019).

[5] Gludovatz,B.et al.A fracture-resistant high-entropy alloy for cryogenic applications.Science 345,1153–1158(2014).

[6] Otto,F.et al.The influences of temperature and microstructure on the tensile properties of a CoCrFeMnNi high-entropy alloy.Acta Mater.61,5743–5755(2013).

ISSN: 2414-1895 DOI: 10.6919/ICJE.202604_12(4).0019

[7] Wang,W.Y.et al.Alloying effects on the mechanical properties and microstructure evolution of Al_xCoCrFeNi high-entropy alloys.Metall.Mater.Trans.A 43,1657–1667(2012).

[8] Ma,S.G.& Zhang,Y.Effect of Nb addition on the microstructure and properties of AlCoCrFeNi high-entropy alloy.Mater.Sci.Eng.A 532,480–486(2012).

[9] Wang,W.R.et al.Effects of Si addition on the microstructure and mechanical properties of Al_xCoCrFeNi high-entropy alloys.Mater.Sci.Eng.A 589,311–318(2014).

[10] He,J.Y.et al.A precipitation-hardened high-entropy alloy with outstanding tensile properties.Acta Mater.102,187–196(2016).

[11] Zhao,Y.Y.,Chen,H.W.,Lu,Z.P.& Nieh,T.G.Thermal stability and coarsening of coherent particles in a precipitation-hardened$(NiCoFeCr)_{94}Ti_2Al_4$ high-entropy alloy.Acta Mater.147,184–194(2018).

[12] Luo,H.,Li,Z.& Raabe,D.Hydrogen enhances strength and ductility of an equiatomic high-entropy alloy.Sci.Rep.7,9892(2017).

[13] Li,Z.,Pradeep,K.G.,Deng,Y.,Raabe,D.& Tasan,C.C.Metastable high-entropy dual-phase alloys overcome the strength–ductility trade-off.Nature 534,227–230(2016).

[14] Zhang,Y.et al.Microstructures and properties of high-entropy alloys.Prog.Mater.Sci.61,1–93(2014).

[15] Senkov,O.N.,Wilks,G.B.,Miracle,D.B.,Chuang,C.P.& Liaw,P.K.Refractory high-entropy alloys.Intermetallics 18,1758–1765(2010).

[16] Tsai,M.H.& Yeh,J.W.High-entropy alloys: a critical review.Mater.Res.Lett.2,107–123(2014).

[17] Wu,Z.,Bei,H.,Pharr,G.M.& George,E.P.Temperature dependence of the mechanical properties of equiatomic solid solution alloys with face-centered cubic crystal structures.Acta Mater.81,428–441(2014)